JACS
JOURNAL OF THE AMERICAN CHEMICAL SOCIETY
Communication
pubs.acs.org/JACS

# Complete Photocatalytic Reduction of $CO_2$ to Methane by $H_2$ under Solar Light Irradiation

Francesc Sastre, Alberto V. Puga, Lichen Liu, Avelino Corma,* and Hermenegildo García*

Instituto Universitario de Tecnología Química CSIC-UPV, Universitat Politècnica de València, Av. De los Naranjos s/n, 46022 Valencia, Spain

Supporting Information

**ABSTRACT:** Nickel supported on silica−alumina is an efficient and reusable photocatalyst for the reduction of $CO_2$ to methane by $H_2$, reaching selectivity above 95% at $CO_2$ conversion over 90%. Although NiO behaves similarly, it undergoes a gradual deactivation upon reuse. About 26% of the photocatalytic activity of Ni/silica−alumina under solar light derives from the visible light photoresponse.

Low-temperature selective reduction of $CO_2$ to methane using solar light is a highly important process that could alleviate the current dependence on fossils fuels and could be neutral from the point of view of climate change and atmospheric $CO_2$ balance.[1−10] Recently we have reported that CO can be either oxidized to $CO_2$ or reduced to $CH_4$ using n-type or p-type metal oxide semiconductors, respectively.[11,12] In particular, and more related to the present work, p-type semiconductors such as NiO, $FeO_x$, CuO, and other transition metal oxides are able to reduce CO to $CH_4$ by water or, more efficiently, by $H_2$ using solar light.[12] Working with 3.5 molar excess of $H_2$, selectivity to $CH_4$ as high as 97% was achieved, at essentially complete CO conversion, using bulk NiO as photocatalyst. Considering the high importance of $CH_4$ as a potential solar fuel and that $CO_2$ is a good feedstock from the environmental point of view and in terms of availability, we have conducted a study on the photocatalytic reduction of $CO_2$ to $CH_4$ by $H_2$ with p-type semiconductors using visible light, according to eq 1.

$$CO_2 + 4H_2 \rightarrow CH_4 + 2H_2O \quad \Delta H_r = -165\ \text{kJ/mol} \tag{1}$$

In a preliminary catalyst study, a series of transition metal oxides were tested for the reduction of $CO_2$ by $H_2$ with simulated sunlight as the source of energy. The results achieved after 1 h reaction time with a conventional solar simulator are presented in Table 1. As can be seen there, while very low conversions were observed for micrometric $Fe_3O_4$ or CuO, other photocatalysts and particularly NiO gave much higher conversions. The series of samples also included Ni supported on silica−alumina ($Ni/SiO_2{\cdot}Al_2O_3$). According to X-ray diffraction (XRD; Figure S1, Supporting Information), this sample contains a mixture of Ni(0) and NiO nanoparticles (NPs). The size distribution of these NPs based on transmission electron microscopy (TEM) is between 7 and 16 nm (Figures S2 and S3); furthermore, both Ni(0) and NiO were found, based on lattice fringes. The role of silica−alumina in this type of heterogeneous catalyst is to increase metal dispersion and stability of the active NPs.

Under the experimental conditions, $Ni/SiO_2{\cdot}Al_2O_3$ gave the highest photocatalytic activity without an apparent relationship with the bandgap of the photocatalyst (see values in Table 1). The products in the gas phase and their distribution depend on $CO_2$ conversion. It was observed that CO appears as a primary but unstable product that converts in a subsequent step into $CH_4$ as a secondary and stable product. Trace amounts of ethane were observed in some cases (see Table 1). It was also noted that the mass balances of carbon, considering exclusively the products in the gas phase, are lower than 100%, especially at higher $CO_2$ conversions.

During the photocatalytic $CO_2$ reduction by $H_2$, the temperature measured at the photocatalyst bed was always lower than 150 °C. We notice that the initial ambient temperature increases rapidly when using $Ni/SiO_2{\cdot}Al_2O_3$ as photocatalyst as $CO_2$ is consumed, reaching a maximum at 140 °C in 15 min when $CO_2$ disappears completely. This should reflect the exothermicity in eq 1. Control experiments in an autoclave showed that, in the dark, using $Ni/SiO_2{\cdot}Al_2O_3$ as catalyst, $CO_2$ reduction by $H_2$ starts to occur at 180 °C, and at this temperature a methane yield of 0.15% at 2.5 h was observed (Figure S4). No temperature increase was recorded in the autoclave at 180 °C, and $CO_2$ conversion was negligible. Notice that the results in Table 1 for $Ni/SiO_2{\cdot}Al_2O_3$ correspond to 15 min. Precedents in the literature report the catalytic thermal reduction of $CO_2$ on Ni−Pt and Ni−Pd alloys performing the reaction at 300 °C, achieving high selectivity toward CO with minor $CH_4$ formation.[14] Thus, all these data support that $CH_4$ formation is a photoactivated and not a thermal process, although it could be accompanied by a thermal catalytic contribution. Additionally, experiments using labeled $^{13}CO_2$ as substrate lead to the formation of $^{13}CH_4$, showing that $CH_4$ is the product of $CO_2$ reduction (see Figure S5 for the relative intensity of the peaks in the $m/z$ range from 10 to 20 amu of the mass spectrum).

Previously we found that, in the photocatalytic reduction of CO, some elemental C can deposit on the photocatalyst surface. In the present case, combustion chemical analyses of the photocatalysts before and after their use reveal that, while the fresh material does not contain a detectable percentage of C

**Received:** January 27, 2014
**Published:** April 11, 2014

 © 2014 American Chemical Society 

**Table 1. Photocatalytic Activity for $CO_2$ Conversion, Including Molar Balances and Selectivities of $CH_4$, CO, and $C_2H_6$, in the Presence of Metal Oxide Semiconductors as Photocatalysts[a]**

| catalyst[b] | particle size (nm) | conversion (%) | molar balance (%)[c] | C (%)[d] | selectivity (%)[c] | | |
|---|---|---|---|---|---|---|---|
| | | | | | $CH_4$ | CO | $C_2H_6$ |
| $TiO_2$ (3.2 eV) | 20−30 | 0 | 99.0 | 0.1 | – | – | – |
| $Ni/SiO_2{\cdot}Al_2O_3$[e] | 7−16 | 94.9 | 89.1 | 1.32 | 97.2 | 2.8 | – |
| NiO (3.5 eV) | 7−30 | 89.8 | 91.9 | 1.6 | 100 | – | – |
| NiO[f] | 12−50 | 15.0 | 89.4 | 1.1 | 88.1 | 11.9 | – |
| NiO[f] | 120−200 | 1.9 | 98.2 | 0.47 | 100 | – | – |
| $Fe_2O_3$ (2.2 eV) | <50 | 51.0 | 99.9 | 0.5 | 4.3 | 95.0 | 0.7 |
| $Fe_3O_4$ | <50 | 12.3 | 99.9 | 0.3 | 0.5 | 96.7 | 2.8 |
| CuO (1.7 eV) | <50 | 0 | 100 | 0.04 | – | – | – |
| CoO (2.6 eV) | <50 | 27.4 | 99.1 | 0.11 | 38.7 | 60.5 | 0.8 |

[a]Irradiation conditions: mixture of $CO_2$ (3.7 mmol, 15%), $H_2$ (17 mmol, 70%), and $N_2$ (3.7 mmol, 15%); irradiation time, 1 h; photocatalyst mass, 250 mg; irradiation source, solar simulator. Blank controls illuminated in the absence of any solid or contacting the solid and gas phase in the dark did not lead to any product. [b]See Supporting Information for the origin and characterization data of these commercially available photocatalysts. The values in parentheses correspond to the reported bandgap energy of the semiconductor in ref 13. [c]Calculated by considering exclusively the products in the gas phase. [d]Weight percentage of carbon on the solid after the photocatalytic experiment determined by combustion chemical analyses. [e]Irradiation time, 0.25 h. [f]Newly synthesized materials; see preparation procedures in the Experimental Details.

by combustion chemical analysis, after photocatalytic reaction a few percent of C is present in the used catalyst (see Table 1). Considering the amounts of deposited carbon, mass balances become satisfactory (>96.6%). In analogous experiments, whereby $CO_2$ and water were submitted to irradiation under otherwise identical conditions, only trace amounts of CO and $CH_4$ were detected after very long irradiation times, indicating that essentially no photocatalytic reforming of carbon takes place under the present conditions.

The benefits of using $Ni/SiO_2{\cdot}Al_2O_3$, combining the photocatalytic activity of NiO with a large surface area support that stabilizes the semiconductor NPs, are revealed by the fact that $Ni/SiO_2{\cdot}Al_2O_3$ exhibits a remarkable reusability that was not achieved with NiO, which undergoes a gradual deactivation upon reuse. Studies on the recyclability of the photocatalysts are presented in Table 2. It can been seen there that $Ni/SiO_2{\cdot}Al_2O_3$ was stable for six uses. Reuses were done by removing the reaction gases and adding fresh $CO_2$ and $H_2$ into the photoreactor at the end of each irradiation time (0.25 h). In contrast, in the case of NiO, a significant decay in the activity was observed. Notice that, in this latter case, regeneration of the catalyst by calcination under air at 450 °C results in a gradual decrease of activity in the first three consecutive cycles, followed by an abrupt deactivation during the fourth use. This is due to the sintering of NiO NPs during the reaction/regeneration cycle, as shown by the decrease in surface area. To support this hypothesis, larger particle sizes of NiO were synthesized and tested (12−50 nm NPs or 120−200 nm hexagonal nanoplates; see the Experimental Details for synthesis and TEM micrographs in Figures S6 and S7, respectively). They led to noticeably lower conversions (15.0 and 1.9% for NiO of 12−50 and 120−200 nm, respectively, see Table 1), thus confirming the influence of particle size on activity. As commented earlier, low $CO_2$ conversion is characterized by product distributions containing a large percentage of CO to the detriment of $CH_4$.

**Table 2. Photocatalytic Activity for $CO_2$ Conversion, Including Molar Balances and Selectivities of $CH_4$, CO, and $C_2H_6$, for Reuses of the Catalyst[a]**

| catalyst | use | conversion (%) | molar balance (%)[d] | selectivity[d] | | |
|---|---|---|---|---|---|---|
| | | | | $CH_4$ | CO | $C_2H_6$ |
| NiO[b] | 1 | 89.8 | 91.9 | 100 | – | – |
| | 2 | 85.1 | 89.5 | 99.2 | – | 0.8 |
| | 3 | 73.9 | 75.3 | 99.7 | – | 0.3 |
| | 4 | 14.4 | 92.3 | 46.8 | 52.2 | 1.0 |
| $Ni/SiO_2{\cdot}Al_2O_3$[c] | 1 | 94.9 | 89.1 | 97.2 | 2.8 | – |
| | 2 | 96.3 | 78.2 | 99.9 | 0.1 | – |
| | 3 | 96.8 | 87.0 | 99.2 | 0.8 | – |
| | 4 | 93.9 | 86.7 | 97.3 | 2.7 | – |
| | 5 | 93.0 | 86.4 | 97.1 | 2.9 | – |
| | 6 | 94.2 | 99.9 | 98.4 | 1.6 | – |

[a]Irradiation conditions: mixture of $CO_2$ (3.7 mmol, 15%), $H_2$ (17 mmol, 70%), and $N_2$ (3.7 mmol, 15%); irradiation time, 1 h; photocatalyst mass, 250 mg; irradiation source, solar simulator. [b]Activation of NiO at 450 °C with air for 5 h. [c]Irradiation time, 0.25 h, adding fresh feed after each run. [d]Calculated by considering exclusively the products in the gas phase.

The above experiments were carried out with simulated sunlight that is known to contain a small percentage of UV light (about 4%). It has been frequently observed that, even though the percentage of UV light in the solar light is low, it can contribute largely or even completely (in the case of $TiO_2$) to the observed overall photocatalytic activity.[15] In order to increase the photocatalytic efficiency, there is an ongoing interest in searching for photocatalysts that are active with visible light. Since NiO has been reported previously to exhibit some visible light photoresponse,[12,16−18] and Ni-based NPs have been shown to display activity for electrocatalytic $CO_2$ reduction,[18,19] it is of interest to assess if the photocatalytic $CO_2$ reduction by $H_2$ can take place to some extent exclusively with visible irradiation on NiO. To investigate this point, we performed a set of irradiations using UV-free light ($\lambda$ > 450 nm; see transmittance spectrum in Figure S8). It was noticed that NiO exhibits some residual photocatalytic activity with visible light irradiation, requiring, however, much longer reaction times. In contrast, as we can see in Table 3, $Ni/SiO_2{\cdot}Al_2O_3$ exhibited a much better visible light photoresponse than NiO, although longer times were needed as compared to UV-containing irradiations. In any case, conversions above 90% with very high selectivity toward $CH_4$ could be obtained using

**Table 3. Photocatalytic Activity for $CO_2$ Conversion, Including Molar Balances and Selectivities of $CH_4$, CO, and $C_2H_6$, under Irradiation with a Solar Simulator Equipped with a Cutoff Filter ($\lambda$ > 450 nm)[a]**

| catalyst | irradiation time (h) | conversion (%) | molar balance (%) | selectivity (%) | | |
|---|---|---|---|---|---|---|
| | | | | $CH_4$ | CO | $C_2H_6$ |
| $Ni/SiO_2 \cdot Al_2O_3$ | 1 | 90.5 | 89.9 | 98.6 | 1.3 | – |
| NiO | 3 | 7.7 | 99.5 | 55.6 | 44.3 | 1.8 |

[a]Irradiation conditions: mixture of $CO_2$ (3.7 mmol, 15%), $H_2$ (17 mmol, 70%), and $N_2$ (3.7 mmol, 15%); photocatalyst mass, 250 mg; irradiation source, solar simulator.

$Ni/SiO_2 \cdot Al_2O_3$ exclusively with visible light. Comparison of the conditions of Table 3 with those of Tables 1 and 2 indicate that, although $Ni/SiO_2 \cdot Al_2O_3$ has visible light photocatalytic activity, about 74% of the response under simulated sunlight irradiation derives from the small UV portion of the spectrum, as estimated by comparing the conversion at 0.25 h with 450 nm cutoff filter (25%) with that obtained using the full wavelength range provided by the solar simulator (94.9%).

The photoaction spectrum of $Ni/SiO_2 \cdot Al_2O_3$ and the apparent quantum yields of the process were determined in the range 350−500 nm using monochromatic light and monitoring the disappearance of $CO_2$ (see Figure S9). The intensity of the monochromatic light was much lower than that under simulated solar light irradiations, and for this reason, the selectivity of the reaction changed and ethylene became the main product. The results show that the photoresponse of the process follows the absorption spectrum of $Ni/SiO_2 \cdot Al_2O_3$ (see also Figure S10), with increasing efficiency going to the UV region, reaching a maximum value of 6%.

With regard to the photocatalytic mechanism, preliminary transient absorption experiments under 355 or 532 nm excitation in acetonitrile suspensions allowed the detection of transients decaying in a few microseconds for $Ni/SiO_2 \cdot Al_2O_3$ (see Figure S11). These transients could be assigned to the charge-separated state, based on quenching by $O_2$ and $CH_3OH$, showing the photoresponse of the material (see Figure S12). We also observed that the temporal profile of the signal was influenced by $H_2$ and, particularly, $CO_2$ purging (see Figure S13), indicating that the monitored transient is sensitive to the presence of these gases.

Considering also the high reduction potential needed for direct electron transfer to $CO_2$ and previous reports on the photocatalytic activity of NiO for water splitting,[20] it seems more reasonable to assume that the process occurs through $H_2$ activation with the formation of Ni−H. Attempts to detect a Ni−H phase by XRD have met with failure, probably due to the high reactivity of NiH with the ambient. Ni−H will be the active $CO_2$ reducing agent, rather than conduction band electrons. Our proposal is summarized in eqs 2 and 3. Ni could activate hydrogen either by reducing $H_2$ to $H^-$ and then reacting with $Ni^+$ or by oxidizing $H_2$ to $H^+$ and then reacting with $Ni^-$. This proposal, based on the formation of metal hydrides, is compatible with the observation of $CH_4$ formation in cases, such as $Fe_2O_3$, where the reduction potential of conduction band electrons is known to be too low to reduce water.

In conclusion, in the present Communication we report a reaction that could potentially impact solar fuel production,

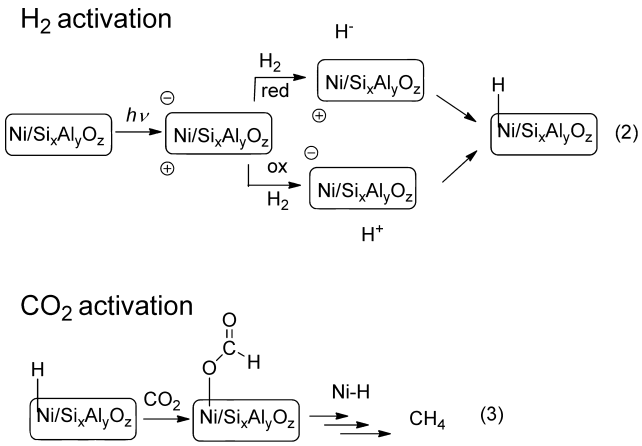


namely the photocatalytic reduction of $CO_2$ to $CH_4$ with sunlight. High conversion and selectivity were achieved in short times using $H_2$ in 4.6 molar excess. An important observation is that the use of a high-surface-area insulating support such as silica−alumina increases the efficiency and durability intrinsic to the photocatalyst, due to an increase in metal dispersion and stability. The reported process can also take place under UV-free visible light.

**Experimental Details.** Photocatalysts were commercial samples, with the exception of NiO samples of 12−50 or 120−200 nm particles. The main textural and analytical data for the commercial photocatalysts are provided in Table S1.

NiO NPs (diameter 12−50 nm) were prepared by a sol−gel method. In a typical synthesis, nickel acetate tetrahydrate (0.5 g) was dissolved in ethanol under constant stirring for 2 h at 40−50 °C, yielding a light greenish sol (50 mL, 0.5 mol/L). An oxalic acid solution (100 mL, 0.23 M in ethanol) was then added slowly to the warm sol to yield a thick greenish gel. The gel product was subsequently dried/digested at 80−110 °C for 24 h and subjected to calcination at 500 °C for 3 h.

NiO nanoplates (diameter 120−200 nm, thickness 20−50 nm) were prepared by a hydrothermal method. Nickel acetate tetrahydrate (0.5 g) was dissolved in water (50 mL). An aqueous NaOH solution (5 mL, 1.25 mol/L) was added dropwise to the nickel acetate solution. After the solution was stirred for 0.5 h, the precipitate thus formed was separated by centrifugation and decantation. The resulting green solid was transferred to an autoclave for hydrothermal treatment at 175 °C for 16 h.

Irradiations in the presence of photocatalysts were carried out spreading uniformly a thin bed of powdered semiconductor previously pelletized into the photoreactor, covering a surface of 1 × 1.5 $cm^2$. The reactor body was made of aluminum to favor heat transfer to the environment, and no special cooling system was used. The temperature and pressure inside the photoreactor were measured by an internal thermocouple and a manometer, respectively. Figure S14 presents two photographs of the photoreactor used and the placement of the photocatalyst and thermocouple. The photoreactor was located 5 cm below the solar simulator beam, and the maximum temperature never increased above 150 °C. $CO_2$ gas diluted with $N_2$ and $H_2$ was introduced into the reactor. Simulated sunlight irradiations of the solids acting as photocatalysts were carried out using a solar simulator (Newport, Oriel Instruments, model 69921) coupled with an AM1.5 filter that provides simulated concentrated sunlight.

The course of the reaction was followed by periodically analyzing the gas phase. At the final time, the possibility of the presence of elemental carbon or organic compounds adsorbed onto the solid was also considered, and the solids were analyzed by combustion chemical analysis (PerkinElmer CHNOS analyzer) or submitted to solid−liquid extraction using dichloromethane as solvent. No products were detected in the extract.

Reproducibility of the data was checked by performing independent experiments in quadruplicate, whereby consistent results were obtained with a dispersion of the conversion and selectivity values less than 5%.

The gas products were analyzed using a Rapid Refinery Gas Analyzer from Bruker that consists of a three-channel gas chromatograph. The first channel analyzes $H_2$ using a micropacket HayeSep Q and Molsieve 5Å column with Ar as carrier gas and TC detector. The second channel analyzes CO, $CO_2$, $N_2$, and $O_2$ with a combination of micropacket Haysep Q, H−N, and Molsieve 13× columns using He as carrier gas and a thermal conductivity detector. The third channel analyzes hydrocarbons from C1 to C5 in an $Al_2O_3$ column with He as carrier gas and a flame ionization detector. The mass balance of each experiment was determined by summing all the moles of the products in the gas phase and dividing by the moles of $CO_2$ converted. Quantification of the moles of the products in the gas phase was carried out considering that $N_2$ remains constant during the experiment and using this gas as internal standard. The response factor of the products with respect to $N_2$ was determined by independent calibrations. Conversion values refer to $CO_2$ and were calculated by dividing the difference between the initial and final moles of $CO_2$ by the initial $CO_2$ moles and then multiplying by 100. Selectivity toward $CH_4$ was calculated by dividing the moles of $CH_4$ formed by the sum of moles of carbon of all the carbon-containing products and then multiplying by 100. Deposition of elemental carbon or the presence of nonvolatile compounds on the solid photocatalyst after irradiation was determined by combustion elemental analysis. The maximum carbon content on the photocatalyst was lower than 2 wt%.

## ■ ASSOCIATED CONTENT

### Ⓢ Supporting Information

Textural data for the commercial oxides; XRD and TEM of commercial $Ni/SiO_2{\cdot}Al_2O_3$; catalytic thermal reaction at various temperatures; mass spectra of the gaseous product from the reaction of $^{13}CO_2$ and $H_2$ on $Ni/SiO_2{\cdot}Al_2O_3$ as compared to that of $CH_4$; TEM of the newly synthesized NiO NPs or nanoplates; photoaction spectrum; absorption spectra of NiO and $Ni/SiO_2{\cdot}Al_2O_3$; transmission spectra for the cutoff filter used to obtain UV-free visible light; transient spectra recorded for $Ni/SiO_2{\cdot}Al_2O_3$; and photographs of the solar simulator and the reactor used. This material is available free of charge via the Internet at http://pubs.acs.org.

## ■ AUTHOR INFORMATION

### Corresponding Authors

acorma@itq.upv.es
hgarcia@qim.upv.es

### Notes

The authors declare no competing financial interest.

## ■ ACKNOWLEDGMENTS

Financial support by the Spanish Ministry of Economy and Competitiveness (Severo Ochoa and CTQ2012-32315) and by the Generalidad Valenciana (Prometeo 2012/013) is gratefully acknowledged. A.V.P. is grateful to both the Consejo Superior de Investigaciones Científicas (CSIC) and the European Social Fund (ESF) for a JAE-Doc postdoctoral grant. Mr. Herme G. Baldoví is thanked for recording the transient spectra and quenching experiments of $Ni/SiO_2{\cdot}Al_2O_3$.

## ■ REFERENCES

(1) Bensaid, S.; Centi, G.; Garrone, E.; Perathoner, S.; Saracco, G. *ChemSusChem* **2012**, *5*, 500−521.
(2) Centi, G.; Quadrelli, E. A.; Perathoner, S. *Energy Environ. Sci.* **2013**, *6*, 1711−1731.
(3) Dey, G. R. *J. Nat. Gas Chem.* **2007**, *16*, 217−226.
(4) Habisreutinger, S. N.; Schmidt-Mende, L.; Stolarczyk, J. K. *Angew. Chem., Int. Ed.* **2013**, *52*, 7372−7408.
(5) Indrakanti, V. P.; Kubicki, J. D.; Schobert, H. H. *Energy Environ. Sci.* **2009**, *2*, 745−758.
(6) Inoue, T.; Fujishima, A.; Konishi, S.; Honda, K. *Nature* **1979**, *277*, 637−638.
(7) Izumi, Y. *Coord. Chem. Rev.* **2013**, *257*, 171−186.
(8) Navalón, S.; Dhakshinamoorthy, A.; Álvaro, M.; Garcia, H. *ChemSusChem* **2013**, *6*, 562−577.
(9) Roy, S. C.; Varghese, O. K.; Paulose, M.; Grimes, C. A. *ACS Nano* **2010**, *4*, 1259−1278.
(10) Wang, C.; Xie, Z.; deKrafft, K. E.; Lin, W. *J. Am. Chem. Soc.* **2011**, *133*, 13445−13454.
(11) Sastre, F.; Oteri, M.; Corma, A.; Garcia, H. *Energy Environ. Sci.* **2013**, *6*, 2211−2215.
(12) Sastre, F.; Corma, A.; García, H. *Angew. Chem., Int. Ed. Engl.* **2013**, *52*, 12983−12987.
(13) Xu, Y.; Schoonen, M. A. A. *Am. Mineral.* **2000**, *85*, 543−556.
(14) Porosoff, M. D.; Chen, J. G. *J. Catal.* **2013**, *301*, 30−37.
(15) Gomes Silva, C.; Juárez, R.; Marino, T.; Molinari, R.; García, H. *J. Am. Chem. Soc.* **2010**, *133*, 595−602.
(16) Jin, Q.; Ikeda, T.; Fujishima, M.; Tada, H. *Chem. Commun.* **2011**, *47*, 8814−8816.
(17) Ni, L.; Tanabe, M.; Irie, H. *Chem. Commun.* **2013**, *49*, 10094−10096.
(18) Shrestha, N. K.; Yang, M.; Nah, Y.-C.; Paramasivam, I.; Schmuki, P. *Electrochem. Commun.* **2010**, *12*, 254−257.
(19) Perez-Cadenas, A. F.; Ros, C. H.; Morales-Torres, S.; Perez-Cadenas, M.; Kooyman, P. J.; Moreno-Castilla, C.; Kapteijn, F. *Carbon* **2013**, *56*, 324−331.
(20) Tong, L.; Iwase, A.; Nattestad, A.; Bach, U.; Weidelener, M.; Gotz, G.; Mishra, A.; Bauerle, P.; Amal, R.; Wallace, G. G.; Mozer, A. J. *Energy Environ. Sci.* **2012**, *5*, 9472−9475.

## ■ NOTE ADDED AFTER ASAP PUBLICATION

The Supporting Information file was replaced in order to include figures that were inadvertently omitted during the revision process. The correct file reposted April 29, 2014